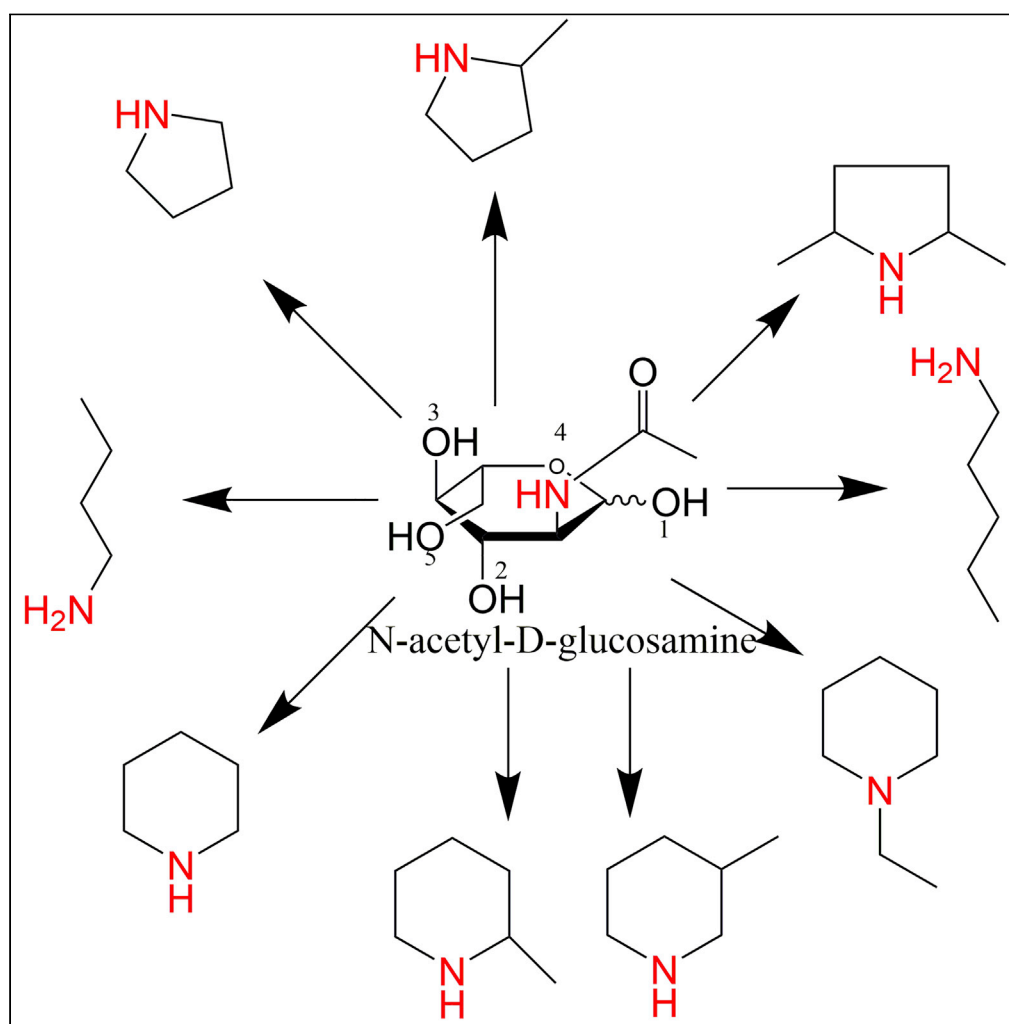# iScience

Article

A Shortcut Route to Close Nitrogen Cycle: Bio-Based Amines Production via Selective Deoxygenation of Chitin Monomers over Ru/C in Acidic Solutions

Shaoqu Xie, Chuhua Jia, Scott Sergio Go Ong, ..., Qiaojuan Wang, Yanhui Yang, Hongfei Lin

hongfei.lin@wsu.edu

HIGHLIGHTS

Utilization of the fixed nitrogen from the ocean

Greener production of amines and ammonium from chitin

Oxygen in glucosamine was removed in the form of H_2O and/or CO/CO_2

Reaction pathways to produce amines from N-acetyl-D-glucosamine (NAG)

Article

A Shortcut Route to Close Nitrogen Cycle: Bio-Based Amines Production via Selective Deoxygenation of Chitin Monomers over Ru/C in Acidic Solutions

Shaoqu Xie,[1] Chuhua Jia,[1] Scott Sergio Go Ong,[1] Ziling Wang,[3] Mei-jun Zhu,[3] Qiaojuan Wang,[4] Yanhui Yang,[4] and Hongfei Lin[1,2,5,*]

SUMMARY

Chitin, a long-chain polymer of N-acetyl-D-glucosamine (NAG) and the most abundant natural nitrogen-containing organic material in the world, is far under-utilized than other biomass resources. Herein, we demonstrate a highly efficient deoxygenation process to convert chitin monomer, i.e., NAG, into various amines, which are the ubiquitous platform chemicals in chemical industry. In the presence of H_2 and Ru/C catalyst, the oxygen atoms in the glucosamine molecules are removed in the form of H_2O and/or CO/CO_2, whereas CO is hydrogenated to CH_4. By optimizing the reaction conditions, $\sim$50% yield of various amines was obtained via the selective deoxygenation of NAG. The reaction mechanism has been proposed. These findings not only promote shell biorefinery in green chemistry and fishery industry but also provide chemicals for material science, resulting in expanding cooperation in new areas such as clean energy, energy conservation, environment protection, and infrastructure.

INTRODUCTION

Amines are ubiquitous platform chemicals in chemical industry due to their lone pair electrons, which make them highly reactive. Amines are widely used in the production of dyes, drugs, pesticides, polymers, etc., as well as in gas treatment such as CO_2 capture (Froidevaux et al., 2016; Hayes, 2001). The common industrial processes for synthesis of amines are the alkylation of ammonia with alcohols or the hydrogenation of nitriles in the presence of a catalyst. Recently, Beller's group found that the metal organic framework-derived cobalt nanoparticles were highly effective for catalyzing the synthesis of amines via reductive amination, which converted aldehydes/ketones with ammonia/amines/nitro compounds to amines with H_2 (Jagadeesh et al., 2017). However, synthesis of amines from ammonia may not be sustainable in that industrial ammonia synthesis is energy intensive and consumes more than 1% of the total energy generated in the world (Winterbottom, 1990). A novel heterogeneously catalyzed process, i.e., reductive aminolysis, was developed for the production of short amines from carbohydrates at low temperatures (Pelckmans et al., 2017). This process, which sacrifices a portion of amines to obtain new amines, does not avoid ammonia synthesis, albeit the utilization of the renewable carbohydrates (Isca and Fernandes, 2018; Song et al., 2017). Nevertheless, production of amines from nitrogen-containing biomass resources is of particular interest and is also critical for sustainability (Froidevaux et al., 2016). Developing highly efficient, safe, atom-economic, and low or non-toxic processes for the production of amines from the nitrogen-containing biomass resources is meaningful for nitrogen recycle.

Cellulose is the most abundant polysaccharide in nature, whereas chitin is the second most abundant one and a major component of the exoskeletons of insects and crustaceans (Omari et al., 2012). Unlike cellulose, chitin is a polymer of the amino sugar N-acetyl-D-glucosamine (NAG). Besides protein and its derivatives, chitin is the most important organic substance having amino groups on its polysaccharide backbone. Although the utilization of biomass resources, such as cellulose (Klemm et al., 2005), hemicellulose (Collard and Blin, 2014), and lignin (Jiang and Hu, 2016), for the production of renewable fuels and chemicals, has been well developed for decades, chitin is far under-utilized when compared with cellulose (Muzzarelli, 1977; Parize et al., 2014; Zargar et al., 2015).

In 2015, Yan and co-workers proposed the concept of "Shell Biorefinery," referring to the fractionation and valorization of crustacean shells and exoskeleton of insects (Yan and Chen, 2015). This commentary article

[1]Gene and Linda Voiland School of Chemical Engineering and Bioengineering, Washington State University, Pullman, WA 99164, USA

[2]Department of Biological Systems Engineering, Washington State University, Pullman, WA 99164, USA

[3]School of Food Science, Washington State University, Pullman, WA 99164, USA

[4]Institute of Advanced Synthesis, School of Chemistry and Molecular Engineering, Jiangsu National Synergetic Innovation Center for Advanced Materials, Nanjing Tech University, Nanjing 211816, China

[5]Lead Contact

*Correspondence: hongfei.lin@wsu.edu

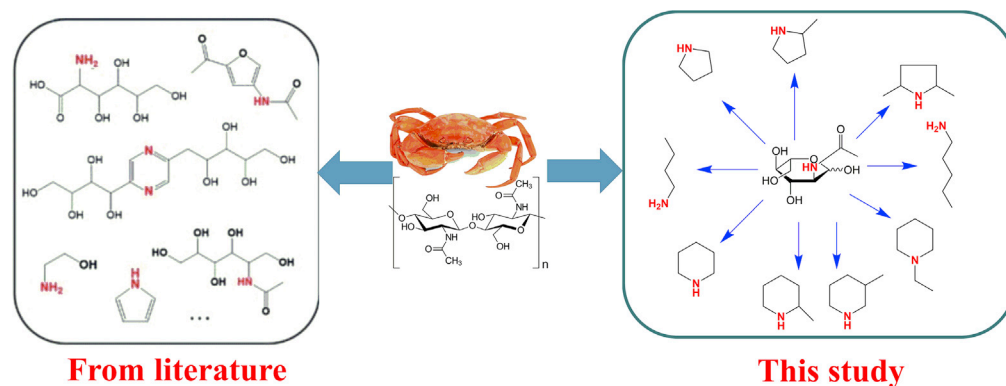https://doi.org/10.1016/j.isci.2020.101096

Figure 1. Shell Biorefinery for the Production of Nitrogen-Containing Chemicals from Chitin
Left: from current literature, Adapted with permission from John Wiley and Sons (Chen and Yan, 2020); right: in this study.

clearly identifies chitin as feedstock for "Nitrogen-rich chemicals for pharmaceuticals, cosmetics, textiles, water treatment, household cleansers, soaps, carbon dioxide sequestration" (Yan and Chen, 2015). In 2016, the same team summarized the overview of the current status of shell biorefinery, pointing out the opportunities of "Shell Biorefinery" for chemicals, porous carbon materials, and functional polymers (Chen et al., 2016). Compared with cellulose, the main difference of chitin is its biologically fixed nitrogen in the side chain. Therefore, as shown in Figure 1 (left), it is possible for chitin to directly derive N-containing chemicals, which, in general, start from highly energy-consuming ammonia synthesis (Chen and Yan, 2020; Rafiqul et al., 2005). The utilization of seafood waste is beneficial not only for environment protection but also for expanding cooperation in new areas such as clean energy, energy conservation, and infrastructure.

Owing to its recalcitrant structure, chitin is hard to be directly converted to other chemicals. Alternatively, after the pretreatment of chitin through acidic or enzymatic hydrolysis (Sashiwa et al., 2003, 2002), the water-soluble monomer, NAG, can be produced. The conversion of NAG to other chemicals has been explored by several groups. For instance, the partial deoxygenation of NAG through pyrolysis generated chemicals, such as 3-acetamidofuran, 3-acetamido-5-acetylfuran (3A5AF), acetamidoacetaldehyde, pyrazines, pyridines, etc., however, in relatively low yields (Chen et al., 1998; Franich et al., 1984). On the other hand, in the presence of Au nanoparticles dispersed on the basic support, the partial oxidation of NAG in water led to the generation of N-acetyl-glucosaminic acid, an α-amino acid with a high yield (95%) (Ohmi et al., 2013). Recently, the emerging processes were developed to convert NAG to platform chemical building blocks in pharmaceutical industry, e.g., 3A5AF, which is used to synthesize the anticancer drug, alkaloid proximicin A (Omari et al., 2012; Sadiq et al., 2018). In the presence of boric acid (B(OH)$_3$) and sodium chloride (NaCl), the yield of 3A5AF increased from 2% (Franich et al., 1984) to 58% (Omari et al., 2012) in dimethylacetamide solvent under microwave irradiation (220°C, 15 min). If the reaction occurred in an imidazolium-based ionic liquid, the yield of 3A5AF would even reach 60% (Drover et al., 2012). However, specialty chemicals such as 3A5AF have a rather small market and can only consume a very limited amount of chitin raw materials.

On the other hand, chitin is a suitable biomass feedstock to produce nitrogen-containing amines. This chitin utilization process may provide a shortcut route to close the nitrogen cycle, avoiding the energy-intensive ammonia synthesis. Although it has been proposed since 2015 to utilize chitin as feedstock for renewable organonitrogen chemicals, few amine compounds with high yields have been achieved. The key challenge is that the amide group easily detaches from the main chain (Bobbink et al., 2015). However, the total deoxygenation of chitin or its monomer NAG is of interest for the synthesis of commodity chemicals such as amines (Chen et al., 1998). To the best of our knowledge, studies on selective deoxygenation of chitin or NAG to amines are very limited. Recently, in a process of transforming chitin to acetic acid, it was found that pyrrole was co-produced at a low yield of 12 mol % (Gao et al., 2016). Hydrogenolysis of NAG over noble metal catalysts produced amide/amino-substituted sugar alcohols, C2–C4 polyols, and N-acetylmonoethanolamine in poor selectivities due to the lack of protecting the amino group of NAG (Bobbink et al., 2015). As a consequence, the deamination dominated, which led to the production of polyols. Thus, the strategy of protecting the amino group must be employed during the conversion of NAG to amines over noble metal catalysts. Herein, we develop a novel catalytic method to produce bio-based amines
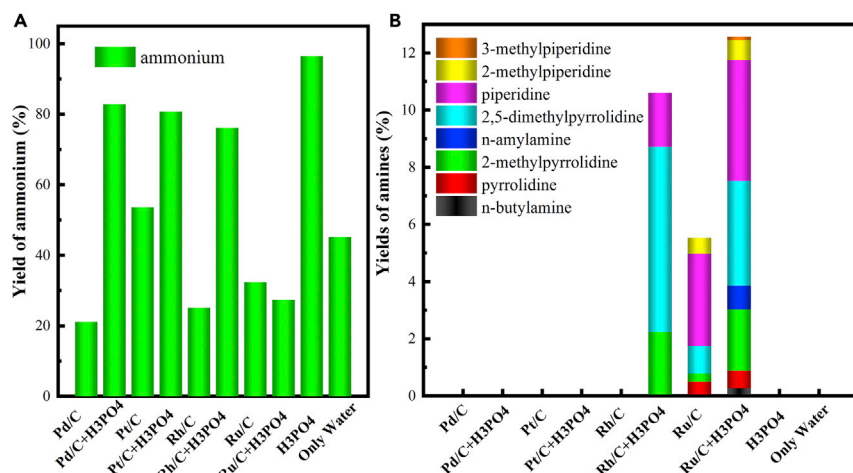
Figure 2. Catalyst Evaluation and Screening

(A and B) Yields of ammonium (A) and amines (B) with various catalysts. Reaction conditions: NAG (0.5 mmol), catalyst (0.03 g), water (5 mL), H_3PO_4 (3 mmol, if applicable), 200°C, 2 h, 28 bar H_2. For all the supported noble metal catalysts, the reactions were carried out with or without the H_3PO_4 co-catalyst. For comparison, two blank experiments without adding a supported noble metal catalyst were the H_3PO_4 + water and the pure water systems.

from NAG by selectively removing the oxygenated group over the supported noble metal catalyst while retaining the amino group in NAG by protonation with an acid co-catalyst, as shown in Figure 1 (right).

RESULTS AND DISCUSSION

Catalyst Screening

In an initial screening, different noble metal catalysts including Pd/C, Pt/C, Rh/C, and Ru/C were employed to conduct the deoxygenation of NAG to produce amines with or without H_3PO_4 in water. Figure 2 shows the different yields of amines and ammonium over these catalysts. In the absence of H_3PO_4, the hydrogenolysis activity of the C–N bond follows the order Pd < Rh < Ru < Pt, which is in agreement with the literature results (Meitzner et al., 1986), as shown in Figure 2A. NAG was very reactive at 200°C, and the amino group was readily cleaved. Deamination was dominant without a catalyst or in the presence of Pd/C or Pt/C, no matter whether H_3PO_4 was present. H_3PO_4 could form the acid-base adduct, and thus the ammonium ions were preserved in the aqueous solution after the reaction. The strategy of protecting amino group against deamination is to reduce the density of the electron cloud, thus leading to lower reactivity. A variety of protective functional groups can be used to bond the amino group by different methods (De Marco et al., 2011). However, harsh reaction conditions such as elevated temperature are usually required later to remove the protective agents and regenerate the products (Sartori et al., 2004; Shivani et al., 2007). Furthermore, the introduction of oxygen-containing moiety as the protective agent is not suitable for our study. However, even with the protective agents, deamination was almost ineluctable over noble metal catalysts at elevated temperatures (Badalcd and Miller, 1970; Barroso and Talati, 2013; Sohn and Ho, 1995). Recently, De Vos and coworkers found that adding H_3PO_4 was beneficial to protect the amino groups (Verduyckt et al., 2017). Indeed, a Brønsted acid can not only hydrolyze NAG to acetic acid and glucosamine but also protonate and protect the amino groups in glucosamine, as shown in Scheme 1. Therefore, it is reasonable to conceive the strategy of protecting the amino groups via protonation to produce amines from selective deoxygenation of NAG. Among our tested noble metal catalysts, the amines were synthesized over the Rh/C and Ru/C catalysts, whereas no amines were produced over the Pd/C and Pt/C catalysts, as shown in Figure 2B. Under acidic conditions, the total yields of the amines were 10.6% and 12.3% with Rh/C and Ru/C, respectively. However, ~76.1% of the amino groups in NAG was removed as ammonium on Rh/C, indicating that the yield of amines could not be further improved remarkably. In contrast, ~ 27.3% of the amino groups in NAG were cleaved with Ru/C so that the yields of amines might be increased by optimizing the reaction conditions. Without adding phosphoric acid, converting NAG over Ru/C could yield ~5.5% amine products, which were only half the yield of amines using the combination of H_3PO_4 and Ru/C. In the latter case, the deamination of glucosamine was much slower. Comparatively, dehydrogenation of the protonated amino group over Pd/C, Pt/C, or Rh/C was proved to be much easier than that over
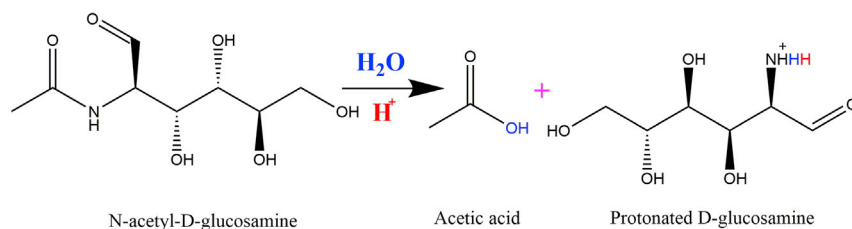
Scheme 1. Protection of Amino Group in the Glucosamine Fragment from N-acetyl-D-glucosamine

Ru/C (Fujii et al., 1991; Verduyckt et al., 2017), and thus with H_3PO_4, deamination was strengthened over Pd/C, Pt/C, or Rh/C, whereas H_3PO_4 kept protecting the amino group in glucosamine over Ru/C. The presence of amino group has promotional effect on Ru-catalyzed hydrogenation and inhibition effects on other metal (Pd, Rh, and Pt)-catalyzed hydrogenation (Deng et al., 2018), thus Ru/C is demonstrated to be superior to Pd/C, Rh/C, and Pt/C in the conversion of NAG in our study.

Owing to the strong polarity of amines, the separation of amines from water is challenging, especially in the presence of mineral acid. Adding a salt (Xie et al., 2017a, 2015a; 2015b, 2013), especially the alkaline salts such as K_2CO_3, as well as a polar organic solvent into the aqueous solution could create a two-phase aqueous system, which may be suitable for the recovery of the polar substance like amines (Fu and Xie, 2019; Xie et al., 2018, 2017b). Herein, acetonitrile and K_2CO_3 were used for recovering the amine products in water. The amines were salted out from the aqueous solution and then extracted into the organic acetonitrile phase, which were then analyzed by gas chromatography coupled with mass spectrometry. The identified amine products include n-butylamine, pyrrolidine, 2-methylpyrrolidine, n-amylamine, 2,5-dimethylpyrrolidine, piperidine, 2-methylpiperidine, 3-methylpiperidine, and 1-ethylpiperidine, as shown in Figure 3. Without adding H_3PO_4, polyols were the main products (Bobbink et al., 2015), whereas the addition of H_3PO_4 not only protected the amino groups but also promoted the dehydration/hydrogenation reactions to produce amine products. As seen in Figure 3, cyclic amines were the main products due to the intramolecular dehydration, whereas the yields of linear aliphatic amines only accounted for <1%. Consequently, pyrrolidine, piperidine, and their derivatives, which hold the stable five-membered or six-membered ring structures (Katritzky et al., 2010; Yoshihiro et al., 2012), were the dominant products.

Besides, NAG underwent deacetylation, and acetic acid was generated. The gas chromatography-thermal conductivity detector analysis of the gaseous products indicates that the reactions involving acetic acid over the different catalysts are different, as shown in Figure S1. On Pd/C, acetic acid decomposed to yield CO_2 and H_2, whereas no CH_4 was detected, which is in agreement with other groups' observation (Bowker et al., 2004) (Figure S1A). Acetic acid reacted over Pt/C involving decarboxylation, decarbonylation, reduction, and esterification (Rachmady and Vannice, 2000), giving CO, CO_2, CH_4, and C_2H_6 as the gaseous products, as shown in Figure S1B. CO is believed to be originated from the decarbonylation of the aldehyde group, which can be further hydrogenated to CH_4 (Davis and Barteau, 1987; Shekhar and Barteau, 1994). With the Ru/C catalyst, acetic acid further went through decarboxylation, decarbonylation, or reduction to form hydrocarbons (CH_4/C_2H_6), acetaldehyde, ethanol, CO, and CO_2 (Santillan-Jimenez and Crocker, 2012). The major deoxygenation routes over Rh/C and Ru/C are decarboxylation and decarbonylation, respectively, as shown in Figures S1C and S1D. On the other hand, ethane was observed due to the consecutive reduction of acetic acid (acetic acid → acetaldehyde → ethanol → ethane). However, on Ru/C, decarbonylation and hydrogenation dominated, and methane was the main final gaseous product.

Effect of Temperature

Owing to the excess hydroxyl groups in D-glucosamine, it is necessary to carry out the reactions at higher reaction temperatures to achieve complete deoxygenation and thus improve the amine yields. As expected, increasing the reaction temperature to 250°C resulted in a remarkable improvement in the selectivity to the cyclic amine products (Figure 4A). However, the nitrogen utilization efficiency for the reaction declined with increasing temperature (Figure 4B). Given the long-enough reaction time, the nitrogen atoms in NAG were completely transformed into the products in the form of amines and ammonium ions at 250°C. Not surprisingly, lowering the reaction temperature to 150°C resulted in yielding no amines, which implied that hydrogenolysis of hydroxyl groups was the necessary step in the conversion of NAG to
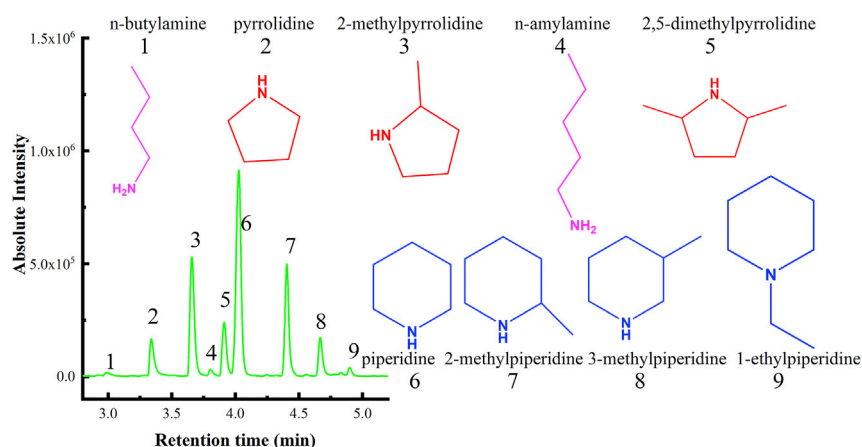
Figure 3. Typical Gas Chromatography Coupled With Mass Spectrometry Chromatogram of the Amine Products in the Salted-Out Organic Phase, and the Confirmed Amine Products from the Deoxygenation of NAG Catalyzed by Ru/C under the Acidic Condition
Reaction condition: NAG (1 mmol), 3 mol % Ru/C, water (5 mL), acid to NAG molar ratio = 4.45, 2 h, 250°C, 33 bar H_2.

amines but could not be fully accomplished at lower temperatures. As seen in Figure S2, alkanolamines were obtained at low temperatures as the hydrogenation activity of Ru/C was the primary factor for obtaining alkanolamines such as 4-hydroxypiperidine and 6-methylpiperidin-3-ol (Geboers et al., 2011a, 2011b; Zhang, 2016). Increasing the reaction temperature led to the production of piperidine and 2-methylpiperidine, instead. By adding 6 molar equivalents of H_3PO_4 with respect to NAG, an overall 44.8% molar yield of the amine products was obtained at 250°C, whereas ~51.0% of the amino group was cleaved to form ammonium ions.

At the elevated temperatures, NAG may undergo complex side reactions, such as glucosamine ring opening, hydrogenolysis, aqueous phase reforming, and water-gas shift reactions (Liang et al., 2014). Over the Ru/C catalyst, glucosamine can be deaminated and subsequently yield polyols via hydrogenolysis (Luo et al., 2007), which was also demonstrated under acid-free condition (Bobbink et al., 2015). The polyols could further decompose to form the gaseous products in the presence of Ru/C (Lahr and Shanks, 2005, 2003; Montassier et al., 1991, 1988). As a consequence, the excessive C-C cleavage dominated with the Ru-catalyzed reaction at elevated temperatures, resulting in a high selectivity to hydrocarbons (mainly methane) (Montassier et al., 1991, 1988), as shown in Figure S3. However, the yields of CO_2 and ethane increased with increasing the temperature due to the decarboxylation and the reduction of acetyl, respectively.

Effect of Phosphoric Acid

H_3PO_4 played an important role in enhancing the yields of amines by protonating the amino group in NAG. In particular, the H_3PO_4 loading has a strong effect on the formation of amines in the deoxygenation process. As seen in Figure 5, when the H_3PO_4 to NAG ratio was 1.48, the overall yield of amines was only 17.3%. Initially, the yields of amines increased with increase in acid loading. As the H_3PO_4 to NAG ratio reached 4.45, the yields of amines reached the maximum at 47.5%, indicating that 4.45 equiv of H_3PO_4 was sufficient to protect the amino groups. The yields of amines changed little when the acid loading, i.e., the acid to NAG molar ratio, was in the range of 4.45–8.0, suggesting that the amino group in the NAG molecule has been fully protected in this acid loading range. Interestingly, NAG tended to form piperidine derivatives with more carbon numbers instead of pyrrolidine with less carbon numbers when increasing the acid loading. Surprisingly, the formation of amines declined with excess acid loading (when the acid to NAG molar ratio was 12). Excessive acid was not favorable for the protection of the amino group due to the high concentration of acid, which may tend to form ammonium phosphate, as shown in Figure S4.

As discussed previously, the deoxygenation of NAG at 200°C was much slower than that at 250°C. The incomplete deoxygenation of NAG yielded a large amount of alkanolamines, which were believed to be the intermediates to amines (Bobbink et al., 2015). The effect of H_3PO_4 loading on the amine yields and distribution at 200°C was shown in Figure S5. The yields of amines were much lower with the insufficient
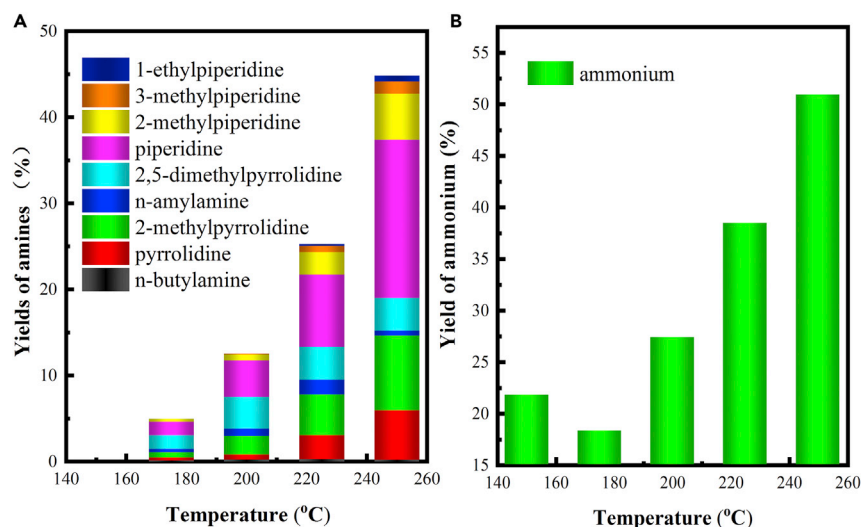
Figure 4. Effect of Reaction Temperature

(A and B) Effects of temperature on the amine yields and distribution (A), and the yield of ammonium ions (B). Reaction condition: NAG (0.5 mmol), 3 mol % Ru/C (0.03 g), water (5 mL), H_3PO_4 (3 mmol), 2 h, 28.2 bar H_2.

or excessive acid loadings than those with the proper H_3PO_4 to NAG molar ratios. Therefore, finely tuning the acid loading was essential to the catalytic deoxygenation process. According to the yields of amines and ammonium ions, the nitrogen balance was satisfying with the different acid loadings under the otherwise identical reaction conditions, indicating that the conversion of NAG was ~100%.

To further demonstrate the role of H_3PO_4, the interactions of H_3PO_4 with NAG and D-glucosamine in the D_2O solution were characterized by the attenuated total reflection Fourier transform infrared (ATR-FTIR) spectroscopy (Okur et al., 2013). The results are shown in Figure 6. It is well known that the adsorption of D_2O is represented by the strong infrared absorbances of O–D stretching at 2,485 cm^{-1} ($\nu(D_2O)$) (Müller et al., 1996). D_2O bending ($\delta(D_2O)$) at 1,206 cm^{-1} is assigned to undissociated D_2O molecules (Belhadj et al., 2015). Figure 6A shows the ATR-FTIR spectra of NAG in pure D_2O and deuterated aqueous solutions with different proportions of H_3PO_4. The NAG molecule consists of a glucosyl group and an amide moiety. As such, the amide functional group is characterized with the bands of the carbonyl stretching, the N-H bending, and the C-N stretching. However, the carbonyl stretching and the N-H bending arise almost exclusively at 1,620 cm^{-1} (Barth and Zscherp, 2002). With the introduction of a small amount of H_3PO_4, the mixture of acid and NAG gave an additional spectrum at 1,019 cm^{-1} that is assigned to the P-O stretch of H_3PO_4 in D_2O (Berry, 1968; Chapman and Thirlwell, 1964). There is no change in intensity of the band of the amide moiety at 1,620 cm^{-1} no matter how the acid to NAG ratio was changed between 1.48 and 11.9, suggesting that there was no interaction between NAG and H_3PO_4 before the hydrolysis of NAG. It seems that that with the addition of H_3PO_4, we cannot tell whether the acid loading is enough to hydrolyze NAG and protect the amino group in D-glucosamine according to the ATR-FTIR spectra of NAG and H_3PO_4 in D_2O at room temperature. Indeed, the preservation of the nitrogen in carbon backbone occurred in the presence of adduct of D-glucosamine and acid, as shown in the Figure 6B. The peak at 1,590 cm^{-1} that represents the N-H bending of the amino group still exists when the H_3PO_4 to D-glucosamine molar ratio is 1.48 or 2.97 and disappears at the H_3PO_4 to D-glucosamine molar ratio of 4.45, indicating that the amino group is completely protonated through the proton transferred from H_3PO_4. The partial protonation of the amino group led to appreciable deamination, as shown in Figure S5. By contrast, the complete protonation of the amino group at the H_3PO_4 to D-glucosamine at molar ratio of 4.45 achieved the highest yields of the amines. The yields of amines are consistent with the extent of the protonation of the amino groups. Therefore, to maximize the yields of amines, the complete protonation of the amino group in glucosamine from NAG is needed.

Other Effects

Figure 7 shows that as the hydrogen pressure increased from 15 to 28.2 bar, the total yield of amines increased remarkably from 9.3% to 47.5%. The yield of each amine increased with increasing the H_2
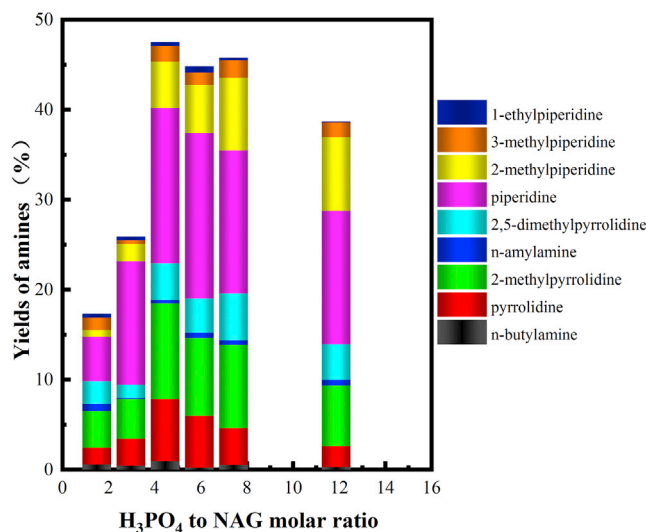
Figure 5. Effect of H$_3$PO$_4$ Loading on the Amine Yields and Distribution at 250°C
Reaction condition: NAG (0.5 mmol), 3 mol % Ru/C (0.03 g), water (5 mL), 2 h, 28.2 bar H$_2$

pressure, which accelerated the hydrogenation rate. Moreover, it appears that increasing the hydrogen pressure to 33 bar led to the highest total yield of amines (∼49.3%). Hydrogen is very important for the deoxygenation of NAG because there are plenty of hydroxyls in NAG molecules. The removal of hydroxyls in the form of H$_2$O was achieved by the hydrogenation. Thus higher H$_2$ pressure led to the removal of more hydroxyls, leading to the final production of amines.

The effects of the NAG concentration are illustrated in Figure 8. Low yields of amines were obtained if the NAG concentration was 0.05 mol/L, which indicates that the amines might undergo a further decomposition. The higher contents of the n-butylamine and pyrrolidine were the evidence for the C-C bond cleavage. However, increasing the NAG concentration to 0.2 and 0.4 mol/L resulted in similar yields of amine as 0.1 mol/L NAG did. Similar to the effect of the acid loading, increasing the NAG concentration was more favorable for the formation of the piperidine derivatives with the six-carbon member ring structure instead of pyrrolidine or 2-methylpyrrolidine with less carbon numbers, which further verified that the amines were more readily decomposed at lower NAG concentrations. However, the highest yields of amines were still obtained when the NAG concentration was 0.1 mol/L.

We have demonstrated the catalytic performance of the Ru/C catalyst in the hydrogenation of NAG. Indeed, a high loading of Ru/C would enhance the catalyst's cracking performance so as to result in the C-N and C-C bonds cleavages (Weng et al., 2016). Measurements on the addition of 1.5 mol% Ru/C catalyst led to much lower amine yields, as the Ru/C was not enough to accelerate the hydrogenation reaction rate (Figure 9). In contrast, the amine yields decreased with increasing the catalyst loading from 3 to 9 mol %, suggesting that the high loading of the Ru/C catalyst promoted the opening of the ring of NAG molecule and further caused the C-C or C-N bond cleavage (Weng et al., 2017), as demonstrated in Figure S6. When the catalyst loading was 9 mol %, more than 90% nitrogen from NAG was removed in the form of ammonium due to the C-N bond cleavage. As a result, 3 mol % Ru/C achieved the highest yields of amines and may prevent the NAG ring from further destruction.

Mechanistic Insights

As previously discussed, the hydrogenation over the catalyst Ru/C not only resulted in amines production but also caused further decomposition of the amines. The time course of product distributions are depicted in Figure 10, and it appears that the results showed good agreement with our prediction. The individual yield of an amine increased first and then decreased due to the decomposition of those amines (Weng et al., 2017). Thus, to reach the highest amine yields (∼50 mol %), H$_3$PO$_4$ to NAG molar ratio of 4.45 and reaction time of 2 h at 250°C and 33 bar H$_2$ were preferred. On the other hand, the overall yield of amines cannot exceed 50% due to the deamination caused by the C-N cracking performance that Ru/C
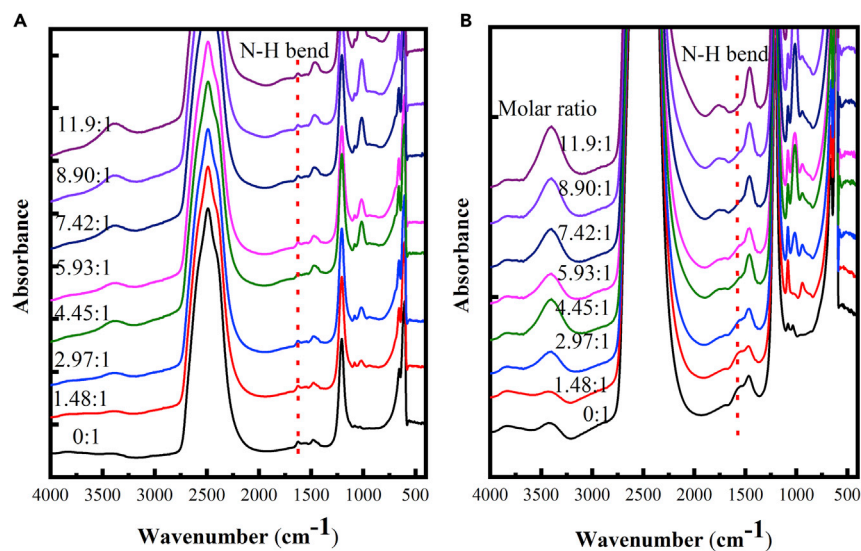
Figure 6. Figure 6 Characterization of Protecting the Amino Group in Glucosamine through ATR-FTIR Spectroscopy

(A and B) Effect of molar ratio of H_3PO_4 to NAG (A) or D-glucosamine (B) on the ATR-FTIR spectra of NAG or D-glucosamine in D_2O at room temperature.

presented at elevated temperatures. To overcome the C-N cracking performance, the effects of reaction time at low reaction temperatures were also investigated, as shown in Figure S7. However, the dehydrogenation rate at 200°C was low, resulting in only 31% amines within 24 h. Increasing the reaction temperature to 225°C led to improvement in the overall yield of amines (43.3%). However, the deamination was also notable. At 250°C, most of the amines decomposed after 24 h reaction, resulting in only a low yield of 13.3% amines (Weng et al., 2017). Therefore it is critical to optimize the reaction time and reaction temperature to maximize the yields of amines.

Herein, we propose a possible mechanism for the deoxygenation of NAG to amines in the presence of H_2 and Ru/C under the acidic condition, as shown in Scheme 2. NAG undergoes hydrolysis first to form acetic acid and D-glucosamine (Bobbink et al., 2015). Then the subsequent protonation of D-glucosamine furnishes the protection of the amino group (Verduyckt et al., 2017). The acetic acid undergoes consecutive reduction to form acetaldehyde, ethanol, and ethane at elevated temperature and under reductive atmosphere (H_2). The majority of acetaldehyde undergoes decarbonylation/hydrogenation to generate methane, which is proved to be the dominant gaseous product. The protonated glucosamine can be reduced to 2-amino-hexan-1,3,4,5,6-pentaol or undergoes decarbonylation to form protonated 5-amino-pentane-1,2,3,4-tetraol. After the cyclization reaction through the intramolecular dehydration, the alkanol-amines are generated as the precursors of amines, albeit at low reaction temperatures. The further removal of hydroxyl functional groups in the alkanolamines enables the production of a range of cyclic amine products at elevated temperatures. In particular, the intramolecular dehydration of 2-amino-hexan-1,3,4,5,6-pentaol, the proton of the amino group reacting with the hydroxyl group at the C6 position, leads to the formation of the piperidine ring with three hydroxyl groups and one hydroxymethyl group. The 2-hydroxymethyl group can be isomerized to 3-hydroxymethyl group at the piperidine ring. When the intramolecular dehydration of 2-amino-hexan-1,3,4,5,6-pentaol occurs at the C5 position of 2-amino-hexan-1,3,4,5,6-pentaol and the proton of the amino group, the ring forming reaction leads to the formation of the pyrrolidine ring with two hydroxyl groups and two hydroxymethyl groups. At last, piperidine, 2-methylpiperidine, 3-methylpiperidine, pyrrolidine, 2-methylpyrrolidine, and 2,5-dimethylpyrrolidine were generated via hydrogenation or decarbonylation. Similarly, the intramolecular dehydration of 5-aminopentane-1,2,3,4-tetraol, together with further hydrogenation or decarbonylation, generated piperidine, pyrrolidine, and its derivatives 2-methylpyrrolidine. Furthermore, 1-ethylpiperidine was obtained from the dehydration between piperidine and ethanol. Aliphatic amines, in just a small quantity, were also obtained from hydrogenation and decarbonylation of 5-aminopentane-1,2,3,4-tetraol.
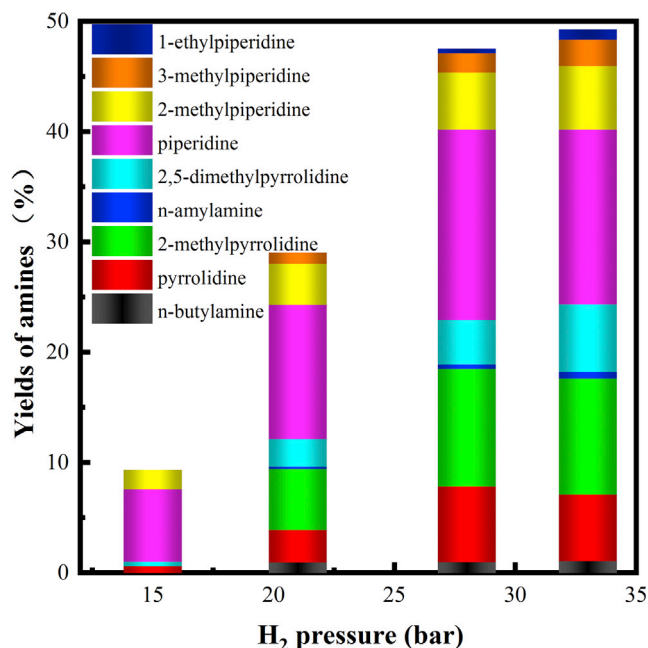
Figure 7. Effect of H₂ Pressure on the Amine Yields and Distribution

Reaction condition: NAG (0.5 mmol), 3 mol % Ru/C (0.03 g), water (5 mL), H_3PO_4 (2.23 mmol), 2 h, 250°C.

The X-ray diffraction (XRD) patterns and transmission electron microscopic images of the fresh and the spent Ru/C catalysts are shown in Figure S8. The major crystalline phases were carbon (graphite structure) and the Ru(101). After one run under different reaction conditions, there are little changes in the XRD patterns of the spent catalysts, implying that the crystallinity of the Ru/C catalyst is almost unchanged. After investigating the metal particle distribution, we observed well-dispersed Ru nanoparticles on the carbon surface, which verifies the high thermal and chemical stabilities of the spent Ru nanoparticles (Figures S8C and S8D) (Weng et al., 2017). However, there are sparse larger Ru particles on the carbon surface due to the aggregation, which may affect the catalytic activity slightly.

Conclusions

Through the controlled hydrogenolysis, the highly efficient deoxygenation of the chitin monomer, NAG, has been demonstrated to produce amines, in which the critical step is to protect the amino group in glucosamine against the deamination. Most of the amino groups will be preserved under the protonation of H_3PO_4. Among Pd/C, Pt/C, Rh/C, and Ru/C, only Rh/C and Ru/C were capable of conducting the deoxygenation of NAG to produce amines. The identified amine products include n-butylamine, pyrrolidine, 2-methylpyrrolidine, n-amylamine, 2,5-dimethylpyrrolidine, piperidine, 2-methylpiperidine, 3-methylpiperidine, and 1-ethylpiperidine, among which cyclic amines dominate. Under the optimized reaction condition, an yield of 50% of different aliphatic amines was obtained from the selective deoxygenation of NAG, whereas the rest of nitrogen in NAG was cleaved to form ammonium ions.

FTIR spectra of glucosamine and H_3PO_4 demonstrated that 4.45 times H_3PO_4 was necessary to protect the amino group in glucosamine to achieve the highest yields of the amines. In the presence of H₂ and the thermally and chemically stable Ru/C catalyst, the oxygen atoms in glucosamine were removed in the form of H_2O and/or CO/CO_2, whereas CO was hydrogenated to CH_4 as the main by-product. Because Ru/C presented C-C cracking and C-N cracking performance, 3 mol % Ru/C achieved the highest yields of amines. The hydrolysis of NAG, the hydrogenation/decarbonylation of glucosamine, the ring-forming step, and removal of hydroxyl groups were proposed as the reaction pathways to produce amines from NAG.

These findings are initial and start a new chapter on the amine production from chitin or its derivatives with biologically fixed nitrogen. Future work will concentrate on the rational design of a new catalyst to improve
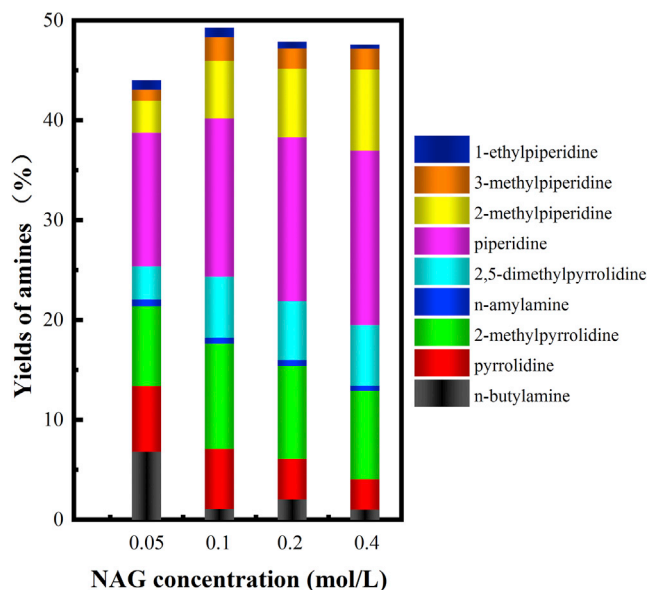
Figure 8. Effect of NAG Concentration on the Amine Yields and Distribution
Reaction condition: 3 mol % Ru/C, water (5 mL), acid to NAG molar ratio = 4.45, 2 h, 250°C, 33 bar H_2.

the selectivity of one specific amine, suppression of the deamination, and the direct conversion of chitin to amines. With such data, the natural nitrogen-based primary and secondary amines from chitin will become a reliable bio-based resource.
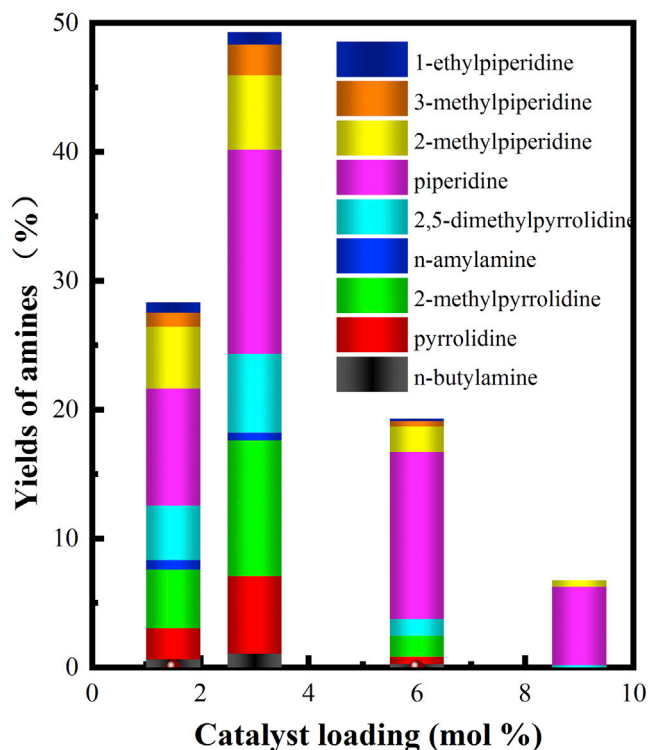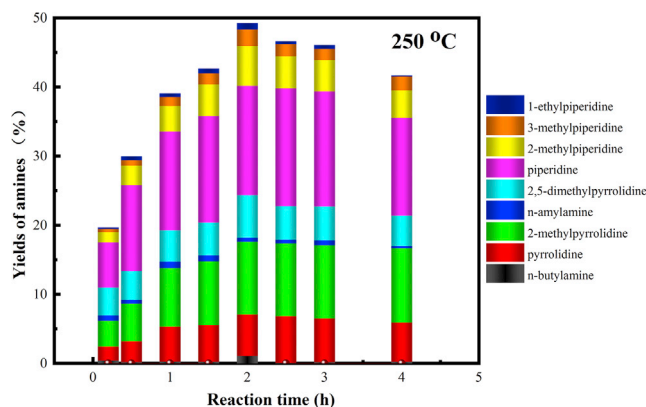

Figure 9. Effects of Catalyst Loading (Based on NAG) on the Amine Yields and Distribution
Reaction condition: NAG (0.5 mmol), water (5 mL), acid to NAG molar ratio = 4.45, 2 h, 250°C, 33 bar H_2.

Figure 10. Effect of Reaction Time on the Amine Yields and Distribution
Reaction condition: NAG (0.5 mmol), 3 mol % Ru/C (0.03 g), water (5 mL), H_3PO_4 (2.23 mmol), 250°C, 33 bar H_2.

Limitations of the Study

This article reports production of amines in deoxygenation of NAG promoted by Ru/C and H_3PO_4. Amine compounds are obtained in ca. 50% N yield along with the formation of ammonium compounds in ca. 50% yield. Among the amines, piperidine is the major product. The selectivity of each amine is not high due to the harsh reaction conditions. Fortunately, separating the amine mixture is not difficult with mature distillation.

Resource Availability

Lead Contact

Further information and requests for resources and reagents should be directed to and will be fulfilled by the Lead Contact, Hongfei Lin (hongfei.lin@wsu.edu).

Materials Availability

This study did not generate new unique reagents.
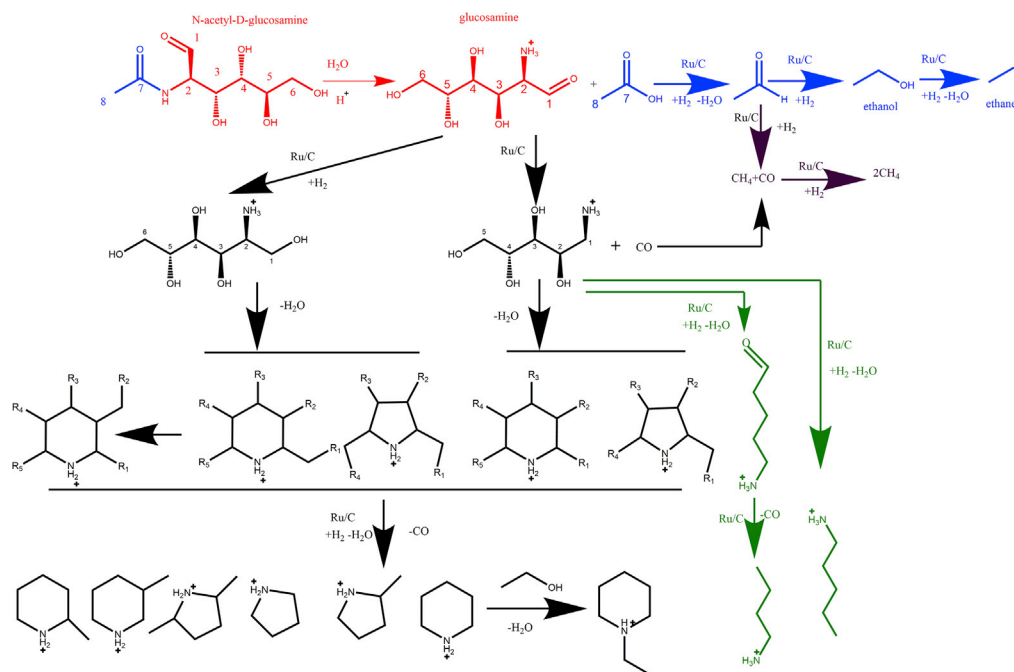
Scheme 2. Proposed Reaction Pathways for the Production of Amines from NAG. R = H or OH Group

METHODS

All methods can be found in the accompanying Transparent Methods supplemental file.

DATA AND CODE AVAILABILITY

Access to data that support the findings of this study are available from the authors on reasonable request.

SUPPLEMENTAL INFORMATION

Supplemental Information can be found online at https://doi.org/10.1016/j.isci.2020.101096.

AUTHOR CONTRIBUTIONS

S.X., C.J., S.S.G.O., and Z.W. designed the experiments and analysis. Q.W. and Y.Y. performed the characterization of the catalysts. S.X. generated all the figures and wrote the manuscript. M.-J.Z. and H.L. critically interpreted and evaluated the data. H.L. supervised all experiments and data analyses, directed the project, and revised the manuscript. All authors read and approved the final version.

DECLARATION OF INTERESTS

The authors declare no competing interests.

REFERENCES

Badalcd, J.L., and Miller, S.L. (1970). The kinetics and mechanism of the reversible nonenzymatic deamination of aspartic Acid1. J. Am. Chem. Soc. https://doi.org/10.1021/ja00712a031.

Barroso, M., and Talati, R. (2013). FRET-based assay for screening modulators of receptor cycling, Unlted States Pat. US 8,283,466 B2. https://doi.org/10.1016/j.(73).

Barth, A., and Zscherp, C. (2002). What vibrations tell us about proteins. Q. Rev. Biophys. 35, 369–430.

Belhadj, H., Hakki, A., Robertson, P.K.J., and Bahnemann, D.W. (2015). In situ ATR-FTIR study of H2O and D2O adsorption on TiO2 under UV irradiation. Phys. Chem. Chem. Phys. 17, 22940–22946.

Berry, E.E. (1968). The infra-red spectrum ef monocalcium phosphate monohydrate. Spectrochim. Acta A Mol. Spectrosc. 24, 1727–1734.

Bobbink, F.D., Zhang, J., Pierson, Y., Chen, X., and Yan, N. (2015). Conversion of chitin derived N-acetyl-d-glucosamine (NAG) into polyols over transition metal catalysts and hydrogen in water. Green. Chem. 17, 1024–1031.

Bowker, M., Morgan, C., and Couves, J. (2004). Acetic acid adsorption and decomposition on Pd(1 1 0). Surf. Sci. 555, 145–156.

Chapman, A.C., and Thirlwell, L.E. (1964). Spectra of phosphorus compounds-I the infra-red spectra of orthophosphates. Spectrochim. Acta 20, 937–947.

Chen, J., Wang, M., and Ho, C.T. (1998). Volatile compounds generated from thermal degradation of N-acetylglucosamine. J. Agric. Food Chem. 46, 3207–3209.

Chen, X., and Yan, N. (2020). Conversion of chitin to nitrogen-containing chemicals. In Chemical Catalysts for Biomass Upgrading, M. Crocker and E. Santillan-jimenez, eds. (Wiley-VCH Verlag GmbH & Co. KGaA), pp. 569–590.

Chen, X., Yang, H., and Yan, N. (2016). Shell biorefinery: dream or reality? Chem. A. Eur. J. https://doi.org/10.1002/chem.201602389.

Collard, F.X., and Blin, J. (2014). A review on pyrolysis of biomass constituents: mechanisms and composition of the products obtained from the conversion of cellulose, hemicelluloses and lignin. Renew. Sustain. Energy Rev. https://doi.org/10.1016/j.rser.2014.06.013.

Davis, J.L., and Barteau, M.A. (1987). Decarbonylation and decomposition pathways of alcohol's on Pd(111). Surf. Sci. 187, 387–406.

De Marco, R., Di Gioia, M.L., Liguori, A., Perri, F., Siciliano, C., and Spinella, M. (2011). N-alkylation of N-arylsulfonyl-α-amino acid methyl esters by trialkyloxonium tetrafluoroborates. Tetrahedron 67, 9708–9714.

Deng, W., Wang, Y., Zhang, S., Gupta, K.M., Hülsey, M.J., Asakura, H., Liu, L., Han, Y., Karp, E.M., Beckham, G.T., et al. (2018). Catalytic amino acid production from biomass-derived intermediates. Proc. Natl. Acad. Sci. U S A 115, 5093–5098.

Drover, M.W., Omari, K.W., Murphy, J.N., and Kerton, F.M. (2012). Formation of a renewable amide, 3-acetamido-5-acetylfuran, via direct conversion of N-acetyl-d-glucosamine. RSC Adv. 2, 4642–4644.

Franich, R.A., Goodin, S.J., and Wilkins, A.L. (1984). Acetamidofurans, acetamidopyrones, and acetamidoacetaldehyde from pyrolysis of chitin and n-acetylglucosamine. J. Anal. Appl. Pyrolysis 7, 91–100.

Froidevaux, V., Negrell, C., Caillol, S., Pascault, J.P., and Boutevin, B. (2016). Biobased amines: from synthesis to polymers; present and future. Chem. Rev. 116, 14181–14224.

Fu, C., and Xie, S. (2019). Salts and 1-propanol induced aqueous two-phase systems: phase separation and application. J. Chem. Technol. Biotechnol. 94, 2372–2381.

Fujii, T., Yukawa, K., and Saito, Y. (1991). Thermal dehydrogenation of cyclooctane by supported noble metal catalysts. Bull. Chem. Soc. Jpn. 64, 938–941.

Gao, X., Chen, X., Zhang, J., Guo, W., Jin, F., and Yan, N. (2016). Transformation of chitin and waste

shrimp shells into acetic acid and pyrrole. ACS Sustain. Chem. Eng. 4, 3912–3920.

Geboers, J., Van De Vyver, S., Carpentier, K., Jacobs, P., and Sels, B. (2011a). Efficient hydrolytic hydrogenation of cellulose in the presence of Ru-loaded zeolites and trace amounts of mineral acid. Chem. Commun. (Camb.) 47, 5590–5592.

Geboers, J.A., Van De Vyver, S., Ooms, R., Op De Beeck, B., Jacobs, P.A., and Sels, B.F. (2011b). Chemocatalytic conversion of cellulose: opportunities, advances and pitfalls. Catal. Sci. Technol. https://doi.org/10.1039/c1cy00093d.

Hayes, K.S. (2001). Industrial processes for manufacturing amines. Appl. Catal. A. Gen. 221, 187–195.

Isca, V.M.S., and Fernandes, A.C. (2018). Direct synthesis of α-aminophosphonates from biomass resources catalyzed by HReO4. Green. Chem. 20, 3242–3245.

Jagadeesh, R.V., Murugesan, K., Alshammari, A.S., Neumann, H., Pohl, M.M., Radnik, J., and Beller, M. (2017). MOF-derived cobalt nanoparticles catalyze a general synthesis of amines. Science 358, 326–332.

Jiang, Z., and Hu, C. (2016). Selective extraction and conversion of lignin in actual biomass to monophenols: a review. J. Energy Chem. https://doi.org/10.1016/j.jechem.2016.10.008.

Katritzky, A., Ramsden, C., Joule, J., and Zhdankin, V. (2010). Handbook of Heterocyclic Chemistry, Handbook of Heterocyclic Chemistry. https://doi.org/10.1016/C2009-0-05547-0.

Klemm, D., Heublein, B., Fink, H.P., and Bohn, A. (2005). Cellulose: fascinating biopolymer and sustainable raw material. Angew. Chem. Int. Ed. https://doi.org/10.1002/anie.200460587.

Lahr, D.G., and Shanks, B.H. (2005). Effect of sulfur and temperature on ruthenium-catalyzed glycerol hydrogenolysis to glycols. J. Catal. 232, 386–394.

Lahr, D.G., and Shanks, B.H. (2003). Kinetic analysis of the hydrogenolysis of lower polyhydric alcohols: glycerol to glycols. Ind. Eng. Chem. Res. 42, 5467–5472.

Liang, G., He, L., Cheng, H., Li, W., Li, X., Zhang, C., Yu, Y., and Zhao, F. (2014). The hydrogenation/dehydrogenation activity of supported Ni catalysts and their effect on hexitols selectivity in hydrolytic hydrogenation of cellulose. J. Catal. 309, 468–476.

Luo, C., Wang, S., and Liu, H. (2007). Cellulose conversion into polyols catalyzed by reversibly formed acids and supported ruthenium clusters in hot water. Angew. Chem. Int. Ed. 46, 7636–7639.

Meitzner, G., Mykytka, W.J., and Sinfelt, J.H. (1986). Metal-catalyzed reactions of methylamine in the presence of hydrogen. J. Catal. 98, 513–521.

Montassier, C., Giraud, D., and Barbier, J. (1988). Polyol conversion by liquid phase heterogeneous catalysis over metals. In Studies in Surface Science and Catalysis, pp. 165–170, https://doi.org/10.1016/S0167-2991(09)60811-9.

Montassier, C., Ménézo, J.C., Hoang, L.C., Renaud, C., and Barbier, J. (1991). Aqueous polyol conversions on ruthenium and on sulfur-modified ruthenium. J. Mol. Catal. 70, 99–110.

Müller, M., Buchet, R., and Fringeli, U.P. (1996). 2D-FTIR ATR spectroscopy of thermo-induced periodic secondary structural changes of poly-(l)-lysine: a cross-correlation analysis of phase-resolved temperature modulation spectra. J. Phys. Chem. 100, 10810–10825.

Muzzarelli, R.A.A. (1977). Chitin Chemistry (Chitin), pp. 87–154, https://doi.org/10.1016/b978-0-08-020367-6.50009-x.

Ohmi, Y., Nishimura, S., and Ebitani, K. (2013). Synthesis of α-amino acids from glucosamine-HCl and its derivatives by aerobic oxidation in water catalyzed by au nanoparticles on basic supports. ChemSusChem 6, 2259–2262.

Okur, H.I., Kherb, J., and Cremer, P.S. (2013). Cations bind only weakly to amides in aqueous solutions. J. Am. Chem. Soc. 135, 5062–5067.

Omari, K.W., Dodot, L., and Kerton, F.M. (2012). A simple one-pot dehydration process to convert N-acetyl-D-glucosamine into a nitrogen-containing compound, 3-acetamido-5-acetylfuran. ChemSusChem 5, 1767–1772.

Parize, P., Billaud, S., Bienvenu, A.L., Bourdy, S., le Pogam, M.A., Reix, P., Picot, S., Robert, R., Lortholary, O., Bouchara, J.P., and Durieu, I. (2014). Impact of Scedosporium apiospermum complex seroprevalence in patients with cystic fibrosis. J. Cyst. Fibros. https://doi.org/10.1016/j.jcf.2014.01.011.

Pelckmans, M., Vermandel, W., Van Waes, F., Moonen, K., and Sels, B.F. (2017). Low-temperature reductive aminolysis of carbohydrates to diamines and aminoalcohols by heterogeneous catalysis. Angew. Chem. Int. Ed. 56, 14540–14544.

Rachmady, W., and Vannice, M.A. (2000). Acetic acid hydrogenation over supported platinum catalysts. J. Catal. 192, 322–334.

Rafiqul, I., Weber, C., Lehmann, B., and Voss, A. (2005). Energy efficiency improvements in ammonia production - perspectives and uncertainties. Energy 30, 2487–2504.

Sadiq, A.D., Chen, X., Yan, N., and Sperry, J. (2018). Towards the shell biorefinery: sustainable synthesis of the anticancer alkaloid proximicin A from chitin. ChemSusChem 11, 532–535.

Santillan-Jimenez, E., and Crocker, M. (2012). Catalytic deoxygenation of fatty acids and their derivatives to hydrocarbon fuels via decarboxylation/decarbonylation. J. Chem. Technol. Biotechnol. https://doi.org/10.1002/jctb.3775.

Sartori, G., Ballini, R., Bigi, F., Bosica, G., Maggi, R., and Righi, P. (2004). Protection (and deprotection) of functional groups in organic synthesis by heterogeneous catalysis. Chem. Rev. https://doi.org/10.1021/cr0200769.

Sashiwa, H., Fujishima, S., Yamano, N., Kawasaki, N., Nakayama, A., Muraki, E., Hiraga, K., Oda, K., and Aiba, S.I. (2002). Production of N-acetyl-D-glucosamine from α-chitin by crude enzymes from Aeromonas hydrophila H-2330. Carbohydr. Res. 337, 761–763.

Sashiwa, H., Fujishima, S., Yamano, N., Kawasaki, N., Nakayama, A., Muraki, E., Sukwattanasinitt, M., Pichyangkura, R., and Aiba, S.I. (2003). Enzymatic production of N-acetyl-D-glucosamine from chitin. Degradation study of N-acetylchitooligosaccharide and the effect of mixing of crude enzymes. Carbohydr. Polym. 51, 391–395.

Shekhar, R., and Barteau, M.A. (1994). Decarbonylation and hydrogenation reactions of allyl alcohol and acrolein on Pd(110). Surf. Sci. 319, 298–314.

Shivani, Gulhane, R., and Chakraborti, A.K. (2007). Zinc perchlorate hexahydrate [Zn(ClO4)2·6H2O] as acylation catalyst for poor nucleophilic phenols, alcohols and amines: scope and limitations. J. Mol. Catal. A. Chem. 264, 208–213.

Sohn, M., and Ho, C.T. (1995). Ammonia generation during thermal degradation of amino acids. J. Agric. Food Chem. 43, 3001–3003.

Song, L., Zheng, M., Pang, J., Sebastian, J., Wang, W., Qu, M., Zhao, J., Wang, X., and Zhang, T. (2017). One-pot synthesis of 2-hydroxymethyl-5-methylpyrazine from renewable 1,3-dihydroxyacetone. Green. Chem. 19, 3515–3519.

Verduyckt, J., Coeck, R., and De Vos, D.E. (2017). Ru-catalyzed hydrogenation-decarbonylation of amino acids to bio-based primary amines. ACS Sustain. Chem. Eng. 5, 3290–3295.

Weng, Y., Qiu, S., Wang, C., Chen, L., Yuan, Z., Ding, M., Zhang, Q., Ma, L., and Wang, T. (2016). Optimization of renewable C5 and C6 alkane production from acidic biomass hydrolysate over Ru/C catalyst. Fuel 170, 77–83.

Weng, Y., Wang, T., Qiu, S., Wang, C., Ma, L., Zhang, Qi, Chen, L., Li, Y., Sun, F., and Zhang, Q. (2017). Aqueous-phase hydrodeoxygenation of biomass sugar alcohol into renewable alkanes over a carbon-supported ruthenium with phosphoric acid catalytic system. ChemCatChem 9, 774–781.

Winterbottom, J.M. (1990). Catalyst handbook. Chem. Eng. Sci. https://doi.org/10.1016/0009-2509(90)80027-c.

Xie, S., Qiu, X., and Yi, C. (2015a). Salting-out effect of tripotassium phosphate on the liquid-liquid equilibria of the (water+acetone+1-butanol+ethanol) system and the salting-out recovery. Fluid Phase Equilib. 386, 7–12.

Xie, S., Yi, C., and Qiu, X. (2015b). Salting-out of acetone, 1-butanol, and ethanol from dilute aqueous solutions. Aiche J. https://doi.org/10.1002/aic.14872.

Xie, S., Song, W., Fu, C., Yi, C., and Qiu, X. (2018). Separation of acetone: from a water miscible system to an efficient aqueous two-phase system. Sep. Purif. Technol. 192, 55–61.

Xie, S., Yi, C., and Qiu, X. (2013). Energy-saving recovery of acetone, butanol, and ethanol from a

prefractionator by the salting-out method. J. Chem. Eng. Data 58, 3297–3303.

Xie, S., Zhang, Y., Yi, C., and Qiu, X. (2017a). Biobutanol recovery from model solutions using potassium pyrophosphate. J. Chem. Technol. Biotechnol. 92, 1229–1235.

Xie, S., Zhang, Y., Zhou, Y., Wang, Z., Yi, C., and Qiu, X. (2017b). Salting-out of bio-based 2,3-butanediol from aqueous solutions. J. Chem. Technol. Biotechnol. 92, 122–132.

Yan, N., and Chen, X. (2015). Sustainability: don't waste seafood waste. Nature. https://doi.org/10.1038/524155a.

Yoshihiro, B., Ryoma, H., and Ryosuke, T. (2012). Heterocyclic compound. Heterocycles 69, 125–126.

Zargar, V., Asghari, M., and Dashti, A. (2015). A review on chitin and chitosan polymers: structure, chemistry, solubility, derivatives, and applications. ChemBioEng. Rev. 2, 204–226.

Zhang, H. (2016). Group decision making based on multiplicative consistent reciprocal preference relations. Fuzzy Sets Syst. 282, 31–46.

Supplemental Information

A Shortcut Route to Close Nitrogen Cycle: Bio-Based

Amines Production via Selective Deoxygenation

of Chitin Monomers over Ru/C in Acidic Solutions

Shaoqu Xie, Chuhua Jia, Scott Sergio Go Ong, Ziling Wang, Mei-jun Zhu, Qiaojuan Wang, Yanhui Yang, and Hongfei Lin

Supporting information

A shortcut route to close nitrogen cycle: bio-based amines production via selective deoxygenation of chitin monomers over Ru/C in acidic solutions

Shaoqu Xie, Chuhua Jia, Scott Sergio Go Ong, Ziling Wang, Mei-jun Zhu, Qiaojuan Wang, Yanhui Yang, Hongfei Lin

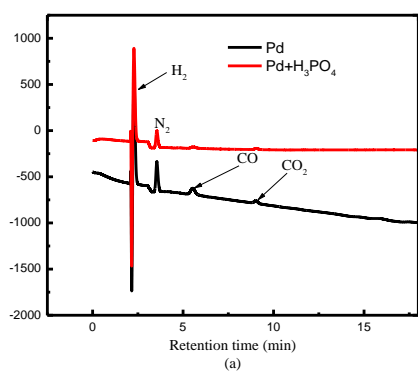Corresponding author: hongfei.lin@wsu.edu (H. Lin).
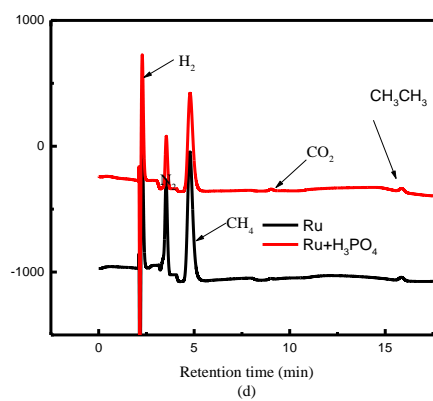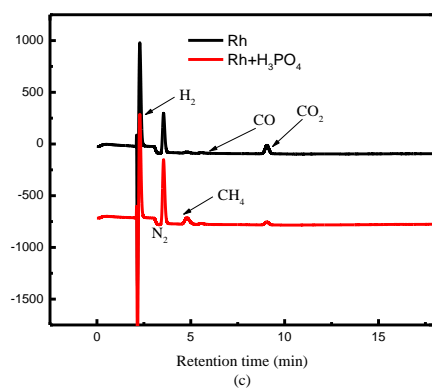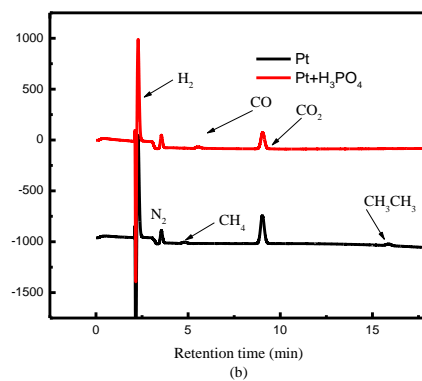
Figure S1 Related to Figure 3, GC-TCD analysis of the gaseous phase after the catalytic reactions (a) Pd-catalyzed reaction, (b) Pt-catalyzed reaction, (c)Rh-catalyzed reaction, (d) Ru-catalyzed reaction.
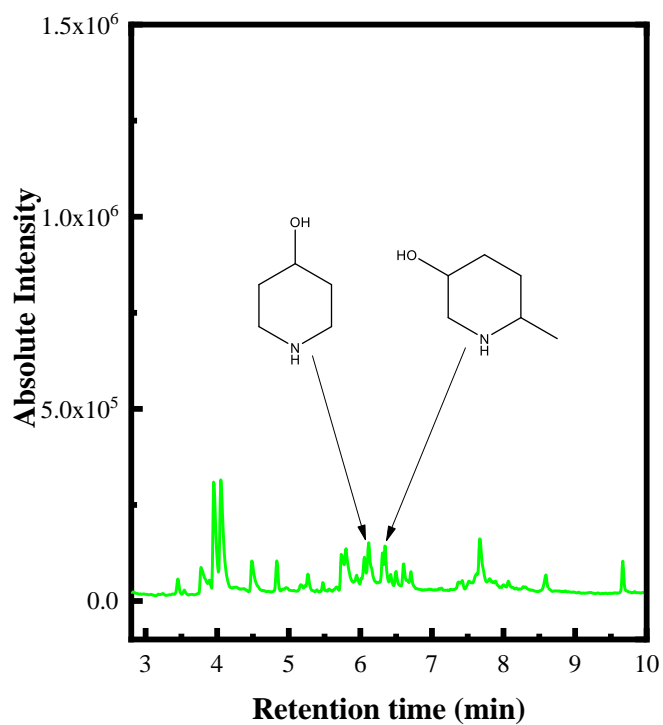
Figure S2 Related to Figure 4, GCMS chromatogram of the products from the conversion of NAG at 200 ºC. Reaction conditions: NAG (0.5 mmol), 3 mol% Ru/C (0.03 g), water (5 mL), H_3PO_4 (3 mmol), 2 h, 28.2 bar H_2.
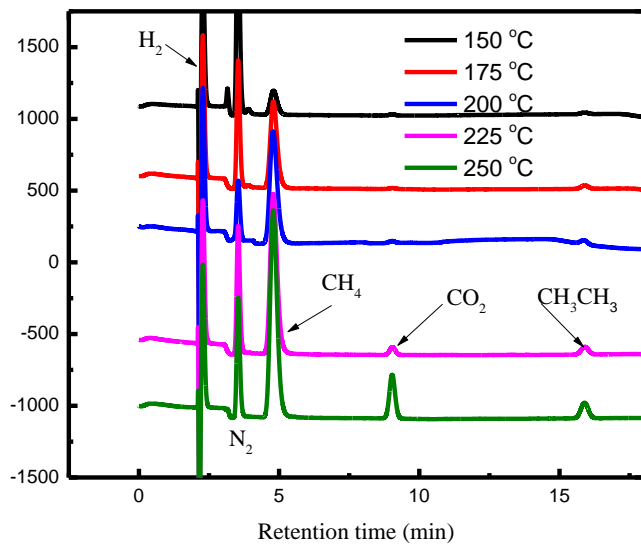
Figure S3 Related to Figure 4, GC-TCD analysis of the gaseous phase after the catalytic reactions. Reaction condition: NAG (0.5 mmol), 3 mol% Ru/C (0.03 g), water (5 mL), H_3PO_4 (3 mmol), 2 h, 28.2 bar H_2.
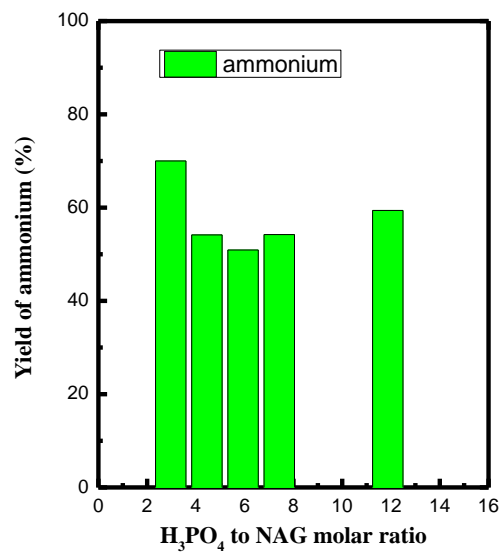
Figure S4 Related to Figure 5, Effects of H3PO4 loading on the yield of ammonium at 250 ºC. Reaction condition: NAG (0.5 mmol), 3 mol% Ru/C (0.03 g), water (5 mL), 2 h, 28.2 bar H$_2$.
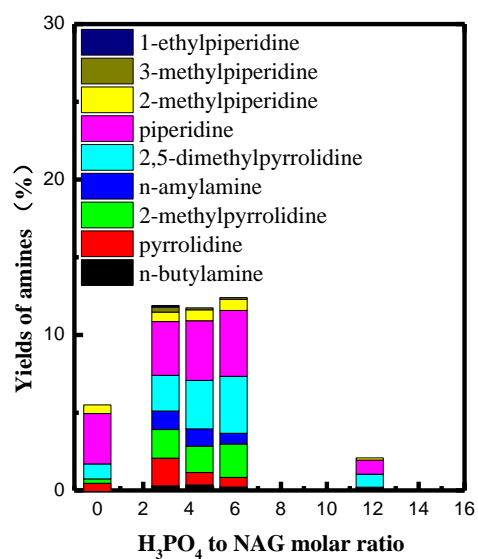
Figure S5 Related to Figure 5, Effect of H₃PO₄ loading on the amines yields and distribution at 200 °C. Reaction condition: NAG (0.5 mmol), 5 % Ru/C (0.03 g), water (5 mL), 2 h, 28.2 bar H₂.
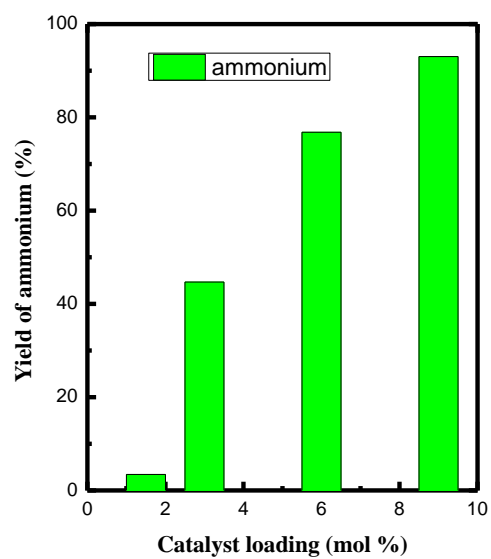
Figure S6 Related to Figure 9, Effects of the Ru/C catalyst loading on the ammonium yield. Reaction condition: NAG (0.5 mmol), water (5 mL), acid to NAG molar ratio=4.45, 2 h, 250 °C, 33 bar H_2.
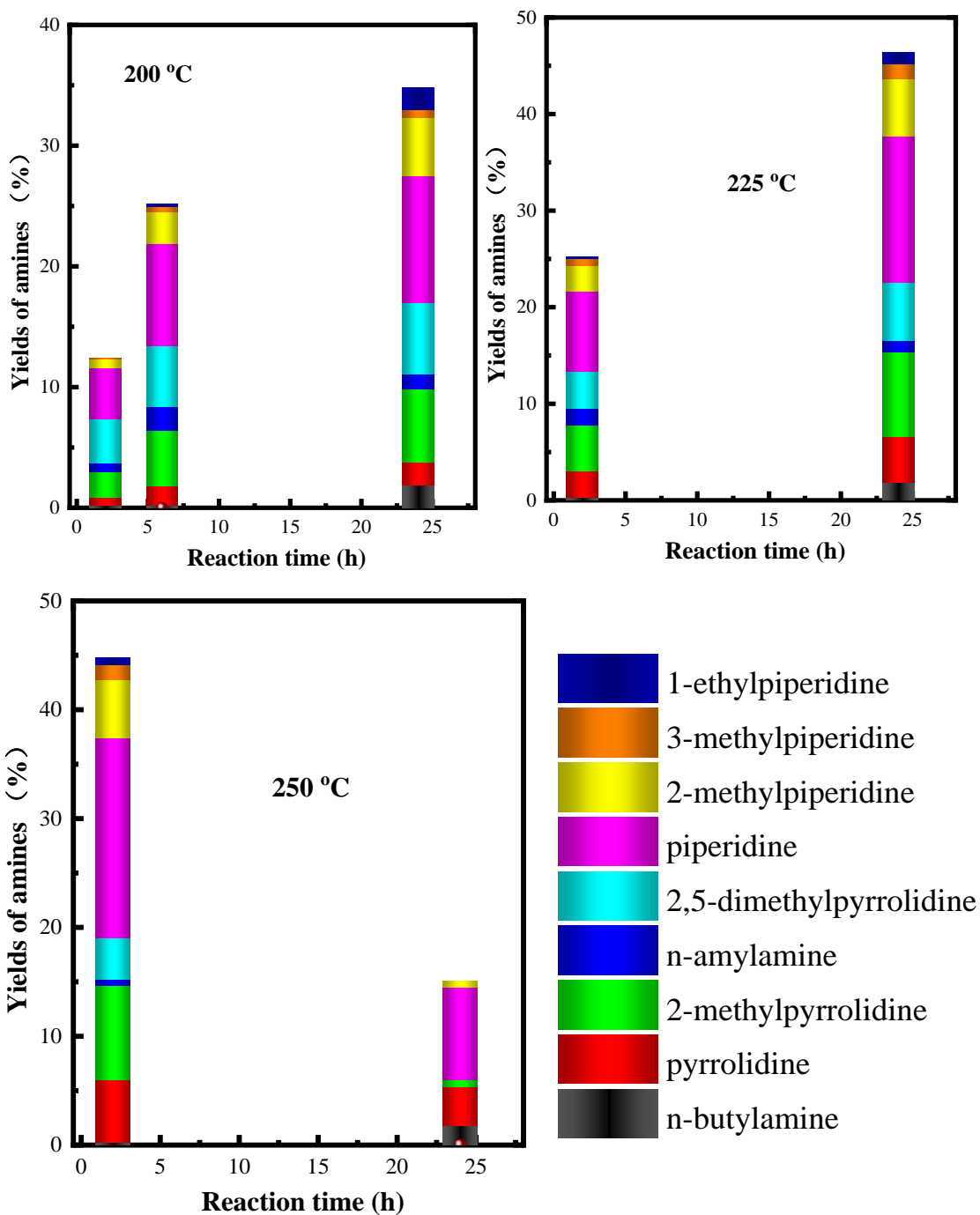
Figure S7 Related to Figure 10, Effect of reaction time on the amines yields and distribution at different temperatures. Reaction condition: NAG (0.5 mmol), 3 mol% Ru/C (0.03 g), water (5 mL), H_3PO_4 (3 mmol), 28.2 bar H_2.
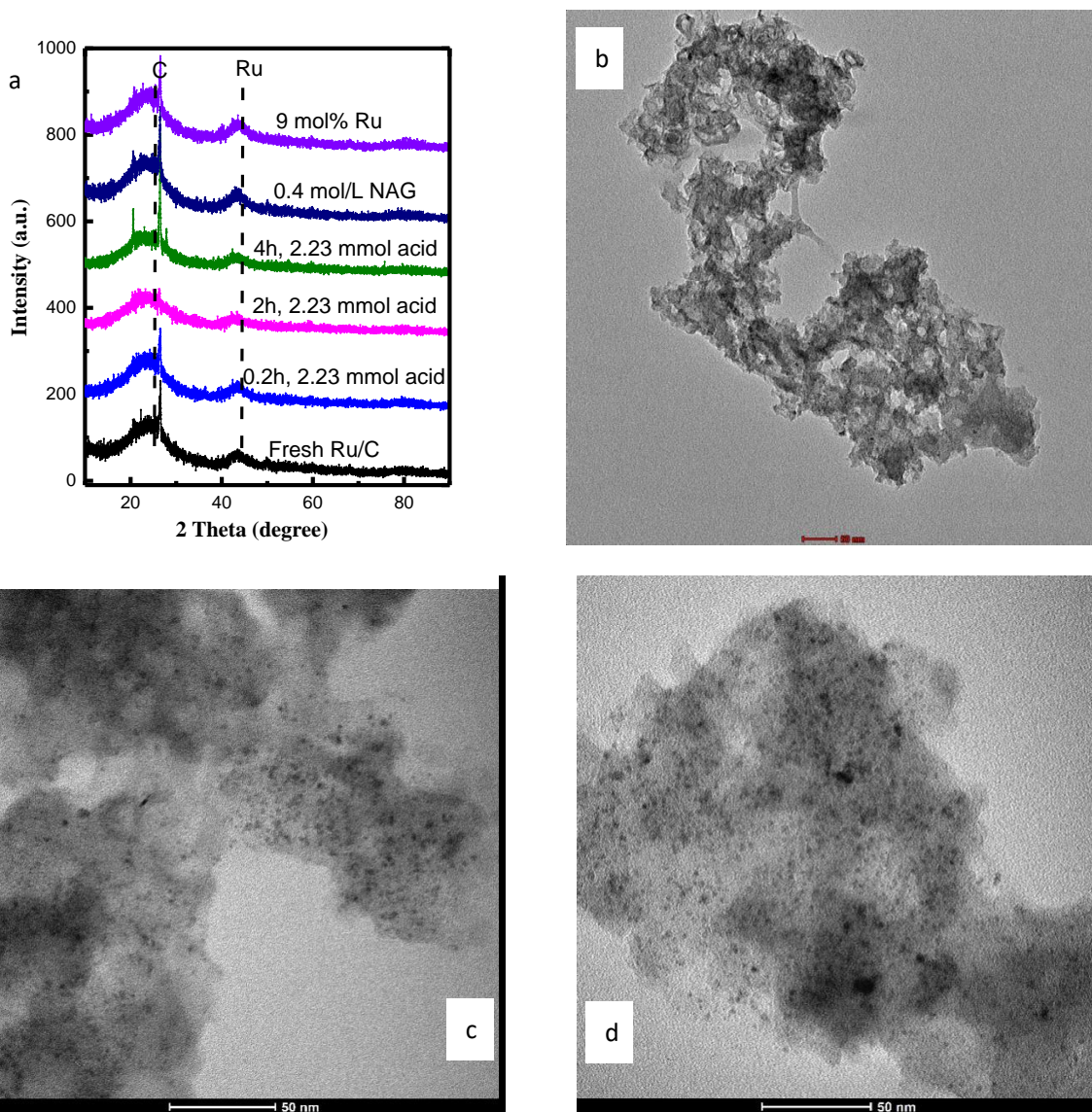
Figure S8 Related to Figure 10, a) XRD spectra of the fresh Ru/C and the spent Ru/C, b) TEM image of fresh Ru/C, c) TEM image of the spent Ru/C at the reaction time of 3h, d) TEM image of the spent Ru/C at the catalyst loading of 9 mol% based on NAG. The scaleplate(b) in red is also 50 nm.

Transparent Methods

Materials

All chemicals were used without further treatment: NAG (≥95.0%, Sigma-Aldrich®), D-Glucosamine hydrochloride (98 %, Alfa Aesar), Pd/C (5 wt%, Sigma-Aldrich®), Ru/C (5 wt%, Sigma-Aldrich®), Pt/C(5 wt%, Sigma-Aldrich®), and Rh/C (5 wt%, Sigma-Aldrich®), sulfuric acid (95~98%, J.T.Baker), acetonitrile (99.9%, J.T.Baker), potassium carbonate anhydrous (99.8%, Fisher Scientific), sodium hydroxide (99.1%, Fisher Scientific), phosphoric acid (85%, aqueous solution, EMD Millipore Corporation, an affiliate of Merck KGaA, Darmstadt, Germany), diethyl ethoxymethylenemalonate (DEEMM, 99%, Sigma-Aldrich®), ammonium hydroxide solution (28% NH_3 in H_2O, ≥ 99.99% trace metals basis, Sigma-Aldrich®), methanol (99.8%, J.T.Baker), sodium borate 10 hydrate (≥99.5%, J.T.Baker), Boric acid (100.4%, Fisher Scientific), deuterium oxide (99.9 atom % D, Sigma-Aldrich®), pyrrolidine (99%, Sigma-Aldrich®), 2,5-dimethylpyrrolidine, (mixture of cis and trans, 93%, , Sigma-Aldrich®), 2-methylpyrrolidine (96%,, Sigma-Aldrich®), piperidine(99%, Sigma-Aldrich®), 2-methylpiperidine (98%, Sigma-Aldrich®.), cis-2,6-dimethylpiperidine (≥97.0%, Sigma-Aldrich®), cyclohexylamine (99.0%, Sigma-Aldrich®), nitrogen and hydrogen (99.999%, A-L Compressed Gases, Inc), ultrapure water (a specific resistance of 18.2 MΩ

cm, prepared through an ultrapure water system, ELGA PURELAB FLEX 2).

2.2 Catalytic Reaction

A Parr Series 5000 Multiple Reactor System with a 4871 temperature controller and six 45 mL vessels was used to carry out the catalytic reactions at elevated pressures and temperatures. Firstly, NAG (0.5 mmol), the catalyst and a magnetic stirrer bar were loaded in a 24 mL quartz liner. Then a certain amount of water and a certain amount of phosphoric acid were also introduced into quartz liners. All the quartz liners were transferred to the vessels of the reactor system for sealing and purging 3 times with 400 psi N_2 followed by 3 times with 400 psi H_2 and refilling with H_2 to the set pressure. The stirring speed of the stirrer bar was fixed at 700 rpm.   Each vessel was individually controlled to reach the desired temperature in 30 mins. After the reaction, the vessels were transferred to the reactor cooling support rack for cooling with cold water.

Analytical methods

Identification of products

After quenching, the reactor was connected to a gas chromatograph (GC) Shimadzu GC-2014, equipped with a thermal conductivity detector (TCD) and a right 12.5 m(L)×0.32mm(ID) packed column which is a combination of 3 m Hayesep D, 4 m HS, and 2.5 m HN and a left 2m (L)×0.32mm(ID) 10% Carbowax 20 m Ch packed column. Ultra-purity N_2, CO_2, CH_4, and H_2 and standard gases containing CO and O_2 were used for the identification of the off-gas.

Before the identification, the solid in the reaction liquid was removed through

filtration and the filtrate was adjusted to alkaline condition and diluted to 50 mL. Potassium carbonate and acetonitrile were utilized to create the liquid-liquid splits where the N-containing chemicals were extracted into the organic phase from a portion of filtrate.(Xie et al., 2017, 2015a, 2015b, 2013) The organic phase was subjected to gas chromatography mass spectrometry analysis (GCMS QP-2020 from Shimadzu, equipped with a Shimadzu SH-Rxi-5SIL MS column (30 m x 0.25 mm ID, 0.25 um film thickness), a flame ionization detector (FID) and a high-performance ion source). The mass spectrum was acquired from 25 m/z to 350 m/z and further resolved by the National Institute of Standards and Technology's (NIST) mass spectral data library. All the products were also confirmed through checking the retention time of the standards on GC-FID.

Quantification of products

The alkaline filtrate was analyzed by a GC Shimadzu GC-2010 equipped with an Agilent J&W CP-Volamine column (30 m, 0.32 mm, 7-inch cage) and an FID. The injector and detector temperatures were fixed at 265 °C. The oven temperature was programmed: initial setting at 90 °C for 20 min, increasing to 265 °C at a program rate of 20 °C/min and holding for 5 min. The calibration curves were prepared by using the standard solutions to quantify the products.

Ammonium content was quantified by using external calibration curve on high performance liquid chromatography HPLC LC-2030 equipped with a C18 column, a UV-Vis Detector and a Refractive Index Detector. The ammonium was derived first by the following reaction in which 300 µL of borate buffer (pH=9), 100 µL of methanol, 44 µL of

deionized water, 6 µL of diethyl ethoxymethylenemalonate (DEEMM), and 30 µL of the

liquid sample were mixed well in a vial.(Kim et al., 2015) The sealed vials were heated at

70 °C in an oven for 2 h to allow complete the derivatization, as well as the degradation of

excess DEEMM(Rebane and Herodes, 2010). After cooling, the ammonium derivatives

were subjected to HPLC analysis at the wavelength of 284 nm. The mobile phase included

mobile phase 1 (HPLC grade acetonitrile) and mobile phase 2 (sodium acetate buffer, 4.84

g of sodium acetate and 2.46 g acetic acid was diluted with water to 4 L). The flow rate

was kept at 1 mL/min, and the flow mode was the gradient elution: 0~2 min, 20%

acetonitrile+80% sodium acetate buffer; 2~32 min, 25% acetonitrile+75% sodium acetate

buffer; 32~40 min, 60% acetonitrile+40% sodium acetate buffer; 40~45 min: 20%

acetonitrile+80% sodium acetate buffer.

The yields of all the products were calculated using the following equations:

$$Product\ Yield\ \% = \frac{mole\ of\ a\ product\ after\ reaction}{mole\ of\ NAG\ before\ reaction}\ X\ 100\ \%$$

In-situ ATR-FTIR analysis

The interaction between phosphoric acid and NAG and the interaction between

phosphoric acid and glucosamine will be revealed by the in-situ FTIR where the change of

the functional groups can be reflected on the spectra.(Shin et al., 1997)   The functional

groups of NAG and glucosamine were analyzed by FTIR spectrophotometry using the

Bruker Tensor II spectrometer equipped with a Harrick Horizon™ and a LN/MCT detector.

The in-situ ATR-FTIR analysis was performed on a 2.89 mL liquid sampling cell

with a Ge horizon trough (HON-LSP-J) where the signals were based on the internal reflectance phenomenon. At first, 0.2212 grams of NAG were dissolved in 10 mL of D_2O, and 0.0662 grams of NAG were dissolved in 3 mL of the 85 % phosphoric acid. Then the two solutions were combined to prepare the NAG solution with varied H_3PO_4 concentrations. The mixtures were dropped on the germanium (Ge) horizon trough for the ATR-FTIR analysis at room temperature. In order to test the interaction between D-glucosamine and H_3PO_4, 0.2194 grams of D-glucosamine hydrochloride and 0.0407 grams of sodium hydroxide were dissolved in 10 mL of D_2O. Different amounts of H_3PO_4 were introduced into the D-glucosamine solution to vary the H_3PO_4 concentration. Similarly, the mixtures were also dropped on the Ge horizon trough for the ATR-FTIR analysis at room temperature. The spectra were obtained with 4 cm^{-1} resolution and 128 scans and the data were saved from 400 to 4000 cm^{-1}.

Catalyst characterization

The transmission electron microscope (TEM) images of the fresh and spent catalysts were captured using a Talos L120C TEM operated at 200 kV. The crystalline structure of the catalysts was characterized by a Rigaku Miniflex 600 XRD powder x-ray diffractometer parameters operated at 40 kV, 15 mA with the following test parameters: scanning between 10° and 90° (2θ) with 0.01° steps and a scanning speed of 5° min^{-1}.

Supplemental References

Kim, Y.H., Kim, H.J., Shin, J.H., Bhatia, S.K., Seo, H.M., Kim, Y.G., Lee, Y.K., Yang, Y.H., Park, K., 2015. Application of diethyl ethoxymethylenemalonate (DEEMM) derivatization for monitoring of lysine decarboxylase activity. J. Mol. Catal. B Enzym. 115, 151–154. https://doi.org/10.1016/j.molcatb.2015.01.018

Rebane, R., Herodes, K., 2010. A sensitive method for free amino acids analysis by liquid chromatography with ultraviolet and mass spectrometric detection using precolumn derivatization with diethyl ethoxymethylenemalonate: Application to the honey analysis. Anal. Chim. Acta 672, 79–84. https://doi.org/10.1016/j.aca.2010.04.014

Shin, S., Jang, J., Yoon, S.H., Mochida, I., 1997. A study on the effect of heat treatment on functional groups of pitch based activated carbon fiber using FTIR. Carbon N. Y. 35, 1739–1743. https://doi.org/10.1016/S0008-6223(97)00132-2

Xie, S., Qiu, X., Yi, C., 2015a. Salting-out effect of tripotassium phosphate on the liquid-liquid equilibria of the (water+acetone+1-butanol+ethanol) system and the salting-out recovery. Fluid Phase Equilib. 386, 7–12. https://doi.org/10.1016/j.fluid.2014.11.013

Xie, S., Yi, C., Qiu, X., 2015b. Salting-out of acetone, 1-butanol, and ethanol from dilute aqueous solutions. AIChE J. https://doi.org/10.1002/aic.14872

Xie, S., Yi, C., Qiu, X., 2013. Energy-saving recovery of acetone, butanol, and ethanol from a prefractionator by the salting-out method. J. Chem. Eng. Data 58, 3297–3303. https://doi.org/10.1021/je400740z

Xie, S., Zhang, Y., Yi, C., Qiu, X., 2017. Biobutanol recovery from model solutions using potassium pyrophosphate. J. Chem. Technol. Biotechnol. 92, 1229–1235. https://doi.org/10.1002/jctb.5113